

Interacting CMEs and their associated flare and SEP activities

A.Shanmugaraju¹ and S.Prasanna Subramanian²

¹Arul Anandar College, Karumathur- 625 514, Madurai Dist., India.

and

²M.K.University College, Aundipatti, Theni Dist., India.

Abstract

We have analyzed a set of 25 interacting events which are associated with the DH type II bursts. These events are selected from the Coronal Mass Ejections (CMEs) observed during the period 1997 – 2010 in SOHO/LASCO and DH type IIs observed in Wind/WAVES. Their pre and primary CMEs from nearby active regions are identified using SOHO/LASCO and EIT images and their height – time diagrams. Their interacting time and height are obtained, and their associated activities, such as, flares and Solar Energetic Particles(>10 pfu) are also investigated. Results from the analysis are: primary CMEs are much faster than the pre-CMEs, their X-ray flares are also stronger (X and M class) compared to the flares (C and M class) of pre-CMEs. Most of the events (22/25) occurred during the period 2000 – 2006. From the observed width and speed of pre and primary CMEs, it is found that the pre-CMEs are found to be less energetic than the primary CMEs. While the primary CMEs are tracked up to the end of LASCO field of view (30Rs), most of the pre-CMEs can be tracked up to <26 Rs. The SEP intensity is found to be related with the integrated flux of X-ray flares associated with the primary CMEs for nine events originating from the western region.

Key words: The Sun – Active Region – Coronal Mass Ejections – Solar Flares – Radio Type II Bursts.

1 Introduction

Coronal Mass Ejection (CME) is the transient ejection of plasma and magnetic fields from the sun's corona into the interplanetary space detected by coronagraphs. CMEs are responsible for large geomagnetic storms and Solar Energetic Particle emission (SEP). Type II radio bursts is an important tool to understand the physical phenomena in the corona of the solar atmosphere and in the interplanetary (IP) medium. CMEs are often associated with Type II radio bursts that are also indicators of coronal and interplanetary shocks. The collision between a slow pre-CME and fast primary CME was reported by Gopalswamy et al. (2001a) and they found radio signatures due to interaction. On the other hand, Lugaz et al.(2005) studied a simulation of interaction between two identical CMEs having same speed in the interplanetary medium. Their simulation results reproduced some general features observed in satellite data for multiple magnetic clouds. Interacting CMEs associated with Type II radio burst cause solar energetic particles as listed by Gopalswamy et al.(2001b). Type II radio burst occurring at all wavelengths from metric to kilometric are associated with most energetic CMEs (Gopalswamy et al.,2005). Long wavelength radio emission in decameter-hectometric (DH) wavelength from 1kHz to 14 MHz frequency range is important to understand the effects of CME in the outer corona and in the IP medium. Also, the radio signatures due to CME interaction are observed in the DH range of spectrum.

Gopalswamy et al.(2002) reported a high correlation between interacting CMEs and SEP association using a set of events during 1996-2001. The emission of non-thermal electrons in the interplanetary medium happens due to interaction between the CMEs. Gopalswamy et al.(2004) emphasized more research on the interacting CMEs because it is important in the concept of space-weather. Recently, Oliverous et al.(2012) have studied an interacting event on 2010 August 01, and suggested that Type II burst radio emission produced is related to CME interaction. The same event is analyzed by Temmer et al.(2012). In their kinematic study, they suggest that the increase in magnetic tension and

pressure when primary CME bends and compress the magnetic field lines of pre-CME, increases the efficiency of drag.

Recently, Prasanna Subramanian and Shanmugaraju (2013) analyzed a set of 15 interacting CMEs from the list of events observed during 1997-2002 by Manoharan et al.(2004). They found existence of relations between interaction height and time delay, and interaction height and frequency of radio emissions. We have extended their study to a wider period during 1997-2010 to identify more events and to complement their results. In this paper, a larger set of 25 interaction events is identified during this period. In addition to the properties of pre and primary CMEs, their associated flare activities are also analyzed.

2 Data Selection

A set of 345 Type II radio bursts in decameter-hectometric (DH) range (listed in Wind/WAVES Type II catalog (http://cdaw.gsfc.nasa.gov/CME_list/radio/waves_type2.html) between 1-14 MHz associated with major flares and CMEs observed during the period 1997-2010 is considered for the present study. The preliminary data of flares and CMEs associated with these events were obtained from the same catalog. Full data corresponding to CMEs are taken from the online catalog http://cdaw.gsfc.gov/CME_list (Yashiro et al., 2004) and X-ray flare data(start time, duration, location, X-ray integrated flux and flare class) are obtained from the website <http://www.ngdc.noaa.gov/stp/spaceweather.html>. The flare-CME association has been examined using the temporal and spatial relationship as given in Harrison (1986, 1995), Jing et al.(2003), Yashiro and Gopalswamy(2008) and Yan et al.(2011). The flare locations and peak flux are also confirmed by both EIT images of SOHO and SDO flare locator images (<http://www.solarmonitor.org/>). The CMEs within one hour duration after flare onset are carefully examined whether they are ejected from that flare location. The CMEs ejected from the same locations are obtained from LASCO coronagraph images and their X-ray flares are obtained from GOES X ray plots.

First, the CMEs causing the IP type II bursts were identified from LASCO C2 and C3 coronagraph observations. For an interacting event, a slow moving CME called pre-CME got interaction with the next or after ejected fast CME, called primary CME. Height-time plots of CMEs are drawn together to see if their trajectories of pre and primary CMEs are intersecting with each other. The height-time plot is extended up to 60 Rs to see any interaction after the LASCO field of view. The interacting CMEs were confirmed with LASCO images of SOHO. Finally, we have selected a set of 25 interacting events based on the following selection criteria: (i) the pre-CMEs ejected before 9 hours from the nearby active region in the same quadrant were identified. (ii) only close events having separation in position angle less than 90° between the events from nearby active region were considered. (iii) primary CMEs associated with DH Type II radio bursts and X-ray flares were considered for the study. (iv) pre-CMEs should be associated with flares and having minimum width 30° were only considered.

The other parameters of CMEs and associated activities are obtained as follows. The time delay of an interacting event is calculated between the onset times of pre and primary CMEs. Some events are found to be associated with major SEP proton events (>10 pfu.) From GOES proton data, we identified 10 major SEP events. SEP data are taken from the website www.umbra.nascom.nasa.gov/sep. The Final Observed Distance (FOD) of all the pre and primary CME events are obtained. If there were more than one preceding CMEs, we considered the pre-CME having more width and less time interval, and it should interact with primary CME as seen in coronagraph observation. All the data (date, time of first detection in LASCO, speed, central position angle (CPA), width and FOD) of pre and primary CMEs are listed in column 2 and 3, respectively in Table 1.

Table 1: Data corresponding to all the pre and primary CMEs observed during the period 1997 – 2010

No.	Pre CME						Primary CME					
	Date	Time	Speed	CPA	Width	FOD	Date	Time	Speed	CPA	Width	FOD
		hh:mm	km/s	deg	deg	Rs		hh:mm	km/s	deg	deg	Rs
1	1997 Nov 06	4:20	307	263	59	12	1997 Nov 06	12:10	1556	Halo	360	25
2	2000 July 22	8:30	204	308	20	5	2000 July 22	11:54	1230	259	229	19
3	2001 Jan 20	19:31	839	Halo	360	25	2001 Jan 20	21:30	1507	Halo	360	28
4	2001 Apr 02	10:06	203	278	36	3	2001 Apr 02	11:26	992	270	80	24
5	2002 Apr 14	4:06	279	311	42	4	2002 Apr 14	7:50	757	323	76	21
6	2003 Mar 18	7:31	619	204	71	4	2003 Mar 18	12:30	1601	263	209	26
7	2003 May 27	23:50	964	Halo	360	17	2003 May 28	0:50	1366	Halo	360	29
8	2003 Nov 18	8:06	1223	144	104	26	2003 Nov 18	8:50	1660	Halo	360	27
9	2003 Dec 2	8:26	240	231	41	4	2003 Dec 2	10:50	1393	261	150	24
10	2004 July 23	17:54	569	260	142	13	2004 July 23	19:31	874	209	100	23
11	2004 July 25	14:30	450	228	45	4	2004 July 25	14:54	1333	Halo	360	21
12	2004 Nov 06	01:31	818	Halo	360	8	2004 Nov 06	2:06	1111	351	214	27
13	2004 Nov 07	14:30	226	286	100	5	2004 Nov 07	16:54	1759	Halo	360	22
14	2004 Dec 29	9:21	345	105	36	14	2004 Dec 29	16:45	774	71	140	25
15	2004 Dec 30	17:54	231	87	54	6	2004 Dec 30	22:30	1035	Halo	360	22
16	2005 Jan 17	9:30	2094	Halo	360	24	2005 Jan 17	9:54	2547	Halo	360	21
17	2005 Jan 20	3:54	205	237	35	4	2005 Jan 20	6:54	882	Halo	360	13
18	2005 June 03	3:32	247	126	128	12	2005 June 03	12:32	1679	Halo	360	23
19	2005 July 07	13:26	432	118	165	16	2005 July 07	17:06	683	Halo	360	13
20	2005 July 13	12:54	471	275	49	8	2005 July 13	14:30	1423	Halo	360	26
21	2005 July 14	7:54	752	266	103	26	2005 July 14	10:54	2115	Halo	360	14
22	2005 July 30	5:57	NA*	75	30	2*	2005 July 30	6:50	1968	Halo	360	26
23	2005 Sep 13	13:24	229	36	40	11	2005 Sep 13	20:00	1866	Halo	360	22
24	2007 June 03	6:54	208	84	36	4	2007 June 03	09:54	467	86	71	8
25	2010 Aug 18	0:24	403	298	88	19	2010 Aug 18	5:48	1471	255	184	25

Table 2: Data of interaction height, time, time delay and details of x-ray flare associated with the primary CMEs.

No.	Date	CME Time	Speed (km/s)	Interaction height (Rs)	Interaction time	Time delay (min)	X-ray Class	Active Region of flare	flare location	Duration of flare (min)	x-ray integrated flux (10^{-2}) J/m ²	SEP Intensity (pfu)
1	1997 Nov 06	12:10	1556	21	14:24	549	X9.4	8100	S18W63	12	36	490
2	2000 July 22	11:54	1230	8	12:30	272	M3.7	9085	N14W56	26	7	17
3	2001 Jan 20	21:30	1507	24	0:00	139	M7.7	9313	S07E46	49	7.2	-
4	2001 Apr 02	11:26	992	6	12:24	144	X.1	9393	N20W70	67	30	-
5	2002 Apr 14	7:50	757	10	9:42	234	C9.6	9893	N19W57	16	0.57	-
6	2003 Mar 18	12:30	1601	27	15:24	301	X1.5	10314	S15W46	39	5.1	-
7	2003 May 28	0:50	1366	28	4:24	85	X3.6	10365	S07W17	33	28	121
8	2003 Nov 18	8:50	1660	8	9:15	28	M3.9	10501	N00E18	47	8.4	-
9	2003 Dec 02	10:50	1393	8	11:52	185	C7.2	10508	S14W70	14	0.51	86
10	2004 July 23	19:31	874	18	22:42	121	C4.1	10652	N04W05	20	0.17	-
11	2004 July 25	14:54	1333	7	15:42	67	M1.1	10652	N08W33	144	6.5	2086
12	2004 Nov 06	2:06	1111	19	4:36	52	M3.6	10696	N09E05	28	5.5	-
13	2004 Nov 07	16:54	1759	5	16:36	330	X2.0	10696	N09W17	33	20	495
14	2004 Dec 29	16:45	774	26	21:00	456	M2.3	10715	N04E62	41	1.8	-
15	2004 Dec 30	22:30	1035	9	23:24	329	M4.2	10715	N04E46	26	3.6	-
16	2005 Jan 17	9:54	2547	*	*	36	X3.8	10720	N15W25	188	84	5040
17	2005 Jan 20	6:54	882	9	7:48	230	X7.1	10720	N14W61	50	130	1680
18	2005 June 03	12:32	1679	15	13:30	604	M1.0	10772	N15E90	54	1.8	-
19	2005 July 07	17:06	683	23	22:30	232	M4.9	10786	N09E03	33	5.3	-
20	2005 July 13	14:30	1423	8	15:18	127	M5.0	10786	N11W90	98	20	134
21	2005 July 14	10:54	2115	23	12:48	205	X1.2	10786	N11W90	73	39	-
22	2005 July 30	06:50	1968	*	*	26	X1.3	10792	N12E60	44	23	-
23	2005 Sep 13	20:00	1866	12	21:00	509	X1.5	10808	S16E39	98	55	-
24	2007 June 03	09:54	469	14	15:00	211	C5.3	10960	S08E67	8	0.12	-
25	2010 Aug 08	05:48	1471	16	7:12	403	C4.5	11099	N18W88	126	2.3	-

*- not possible to measure

Table 3: Details of X-ray flare class of Pre-CMEs.

No.	Date	CME Time	X-ray Class	Active Region of flare	flare location	Duration of flare (min)	x-ray integrated flux (10^{-2} J/m ²)
1	1997 Nov 06	4:20	C1.9	8100	S15W56	29	0.28
2	2000 July 22	8:30	M1.0	9090	N12W05	32	1.4
3	2001 Jan 20	19:31	M1.2	9313	S07E40	26	1.2
4	2001 Apr 02	10:06	M1.9	9393	N17W60	14	1.3
5	2002 Apr 14	4:06	M1.4	9893	N22W45	48	3.2
6	2003 Mar 18	7:31	C2.1	10314	S15W45	32	0.24
7	2003 May 27	23:50	X1.3	10365	S07W17	17	7.1
8	2003 Nov 18	8:06	M2.3	10501	N00E18	39	5.1
9	2003 Dec 02	8:26	C3.9	10508	SW	20	0.37
10	2004 July 23	17:54	M2.2	10652	N04W08	32	1.5
11	2004 July 25	14:30	M2.2	10652	N04W30	18	1.3
12	2004 Nov 06	1:31	M5.9	10696	NE	26	8.5
13	2004 Nov 07	14:30	C7.0	10696	N08W14	22	0.63
14	2004 Dec 29	9:21	C2.6	10713	NE	119	1.2
15	2004 Dec 30	17:54	B5.1	10715	N03E49	7	0.017
16	2005 Jan 17	9:30	X2.0	NA	N13W19	NA	NA
17	2005 Jan 20	3:54	C4.8	10720	N19W58	15	0.27
18	2005 June 03	3:32	C3.1	10772	S17E21	45	0.45
19	2005 July 07	13:26	C2.6	10789	N17E48	37	0.48
20	2005 July 13	12:54	M3.2	10786	N08W79	21	1.3
21	2005 July 14	7:54	M9.1	10786	N09W90	106	8.4
22	2005 July 30	5:57	C9.4	10792	N11E53	33	1.1
23	2005 Sep 13	13:54	C4.5	10808	SE	42	0.95
24	2007 June 03	6:54	M4.5	10960	S06E63	7	0.93
25	2010 Aug 18	00:54	C1.5	11099	NW	77	0.54

3 Results

For example, a C class flare observed from the active region 10696 in the location N08W14 is shown in the left panel of Figure 1a. Right panel shows a pre-CME ejected at 14:30UT on 07 November 2004 with a speed 226 km/s and width 100° at position angle 286° . An X class flare is associated with the primary CME shown in left panel of Figure 1b from the active region 10696 in the location N09W17. A halo primary CME at 16:54 UT

with speed 1759 km/s and width 360° is shown in the Fig. 1b (right panel). Around 17:00 UT, the primary CME interacted with the pre-CME. Radio type II bursts observed in the Wind/WAVES dynamic spectrum below 14 MHz corresponding to the primary CME is shown in Fig.2. It is reported that the frequency range of this DH type II is 14 MHz – 60 kHz during the interval 16:25 UT on 7 November to 20:00 UT of next day. Fig.3 shows X-ray flare profile associated with the pre and primary CMEs. It seems that the flare associated with pre-CME have peak X-ray flux C7.0 at 14:06 UT and the flare associated with primary CME have peak X-ray flux X2.0 at 16:06 UT . Fig.4 shows the height-time diagram of both the CMEs in which the interaction is seen $\sim 17:00$ UT around a height of 5 to 7 Rs. At this time of interaction, the position of leading edges of these two CMEs are reported as pre-CME = 6 Rs and primary CME = 7Rs.

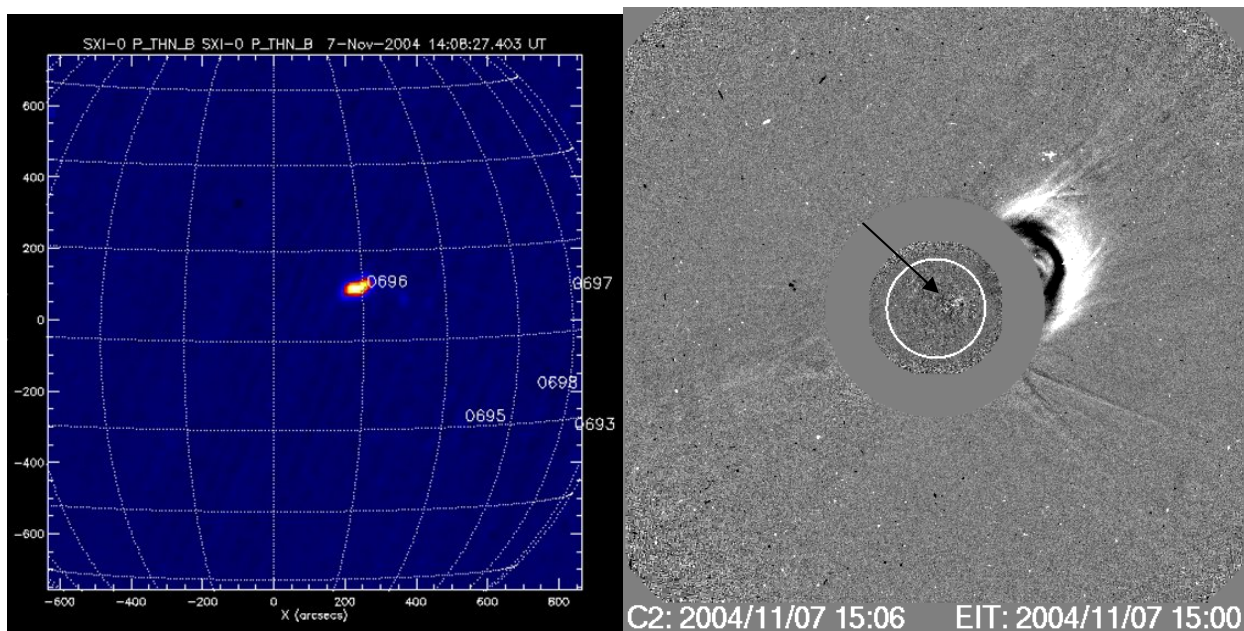


Fig.1a C class flare ejected from the active region 10696 at the location N08W14 is shown (SXI image) in the left panel. The pre-CME ejected at 14:30UT (speed=226 km/s, CPA= 286° , width= 100°) is shown (C2 coronagraph picture) in the right panel. The arrow mark indicates the active region of flare at which the pre-CME ejected.

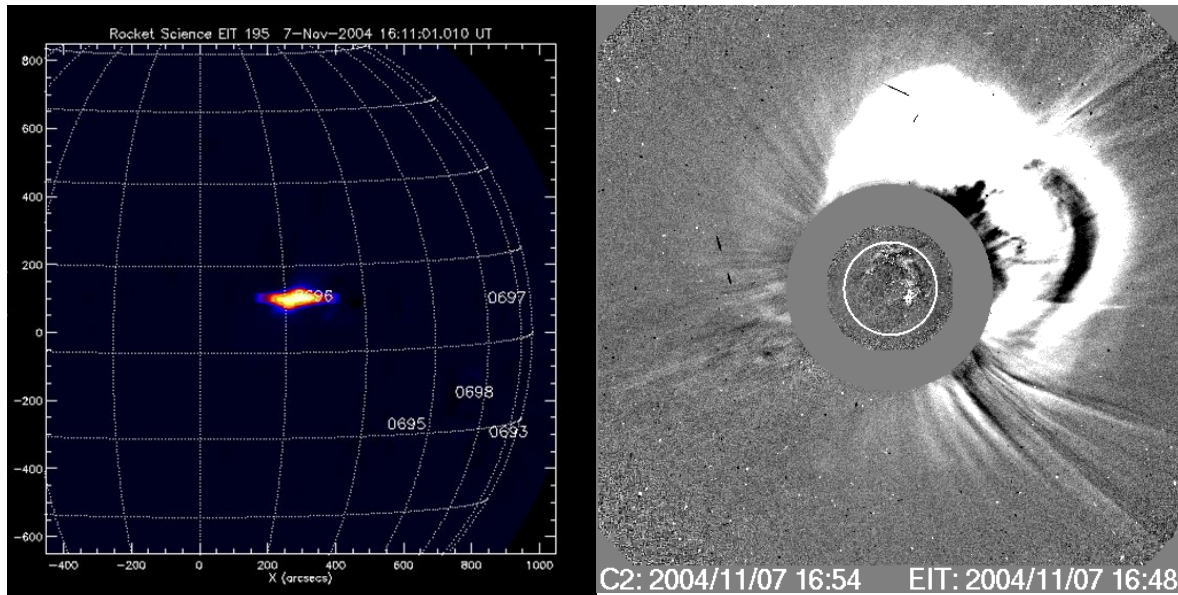


Fig. 1b X class flare ejected from the active region 10696 at the location N09W17 is shown in the left panel. The primary CME ejected at 16:54UT (speed=1759 km/s, width=360°) is shown (C2 coronagraph picture) in the right panel. The mean position angle of the pre- CME is 298° and primary CME is 360°. Interaction of the two CMEs occurred ~17:00 UT around a height of ~5 Rs is seen on the right panel.

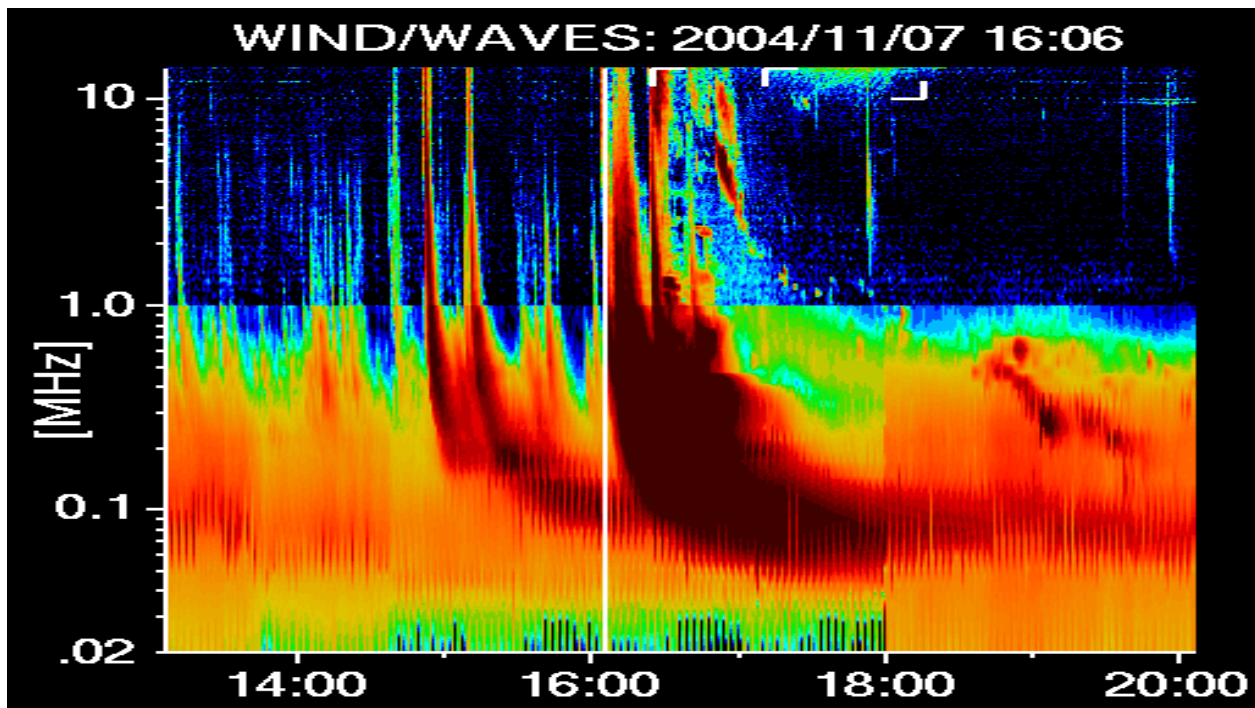


Fig. 2 DH type II burst recorded by Wind/Waves on 7 November 2004. The radio burst started around 14 MHz at 16:25 UT.

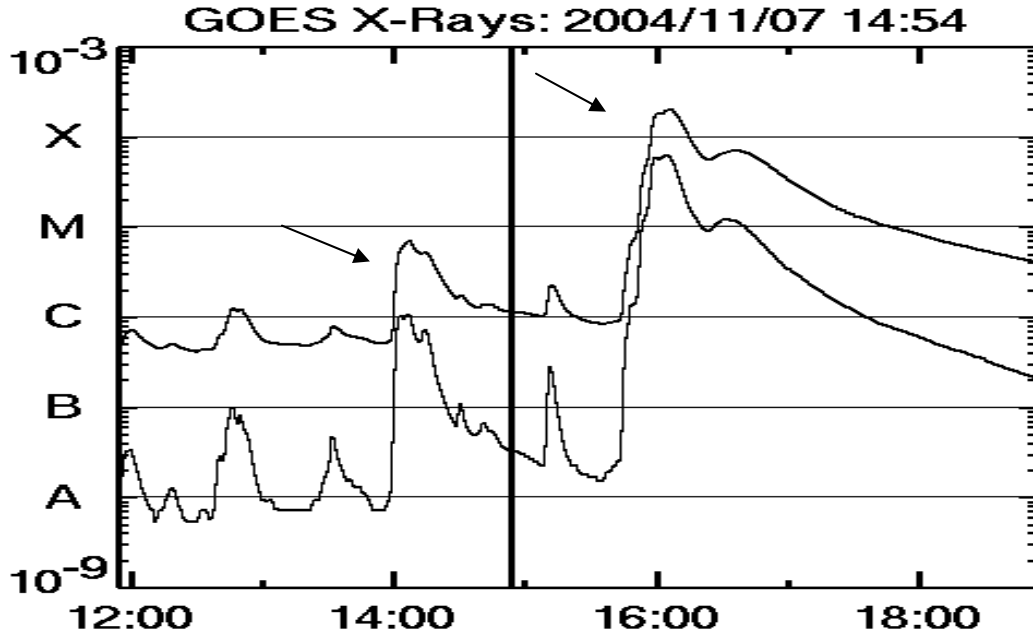


Fig. 3 GOES X-Ray flare profiles on 07 November 2004. The left arrow shows a C-class flare associated with pre-CME and the right arrow shows an X-class flare associated with the primary CME. The vertical line denotes the time of observation 14:54UT.

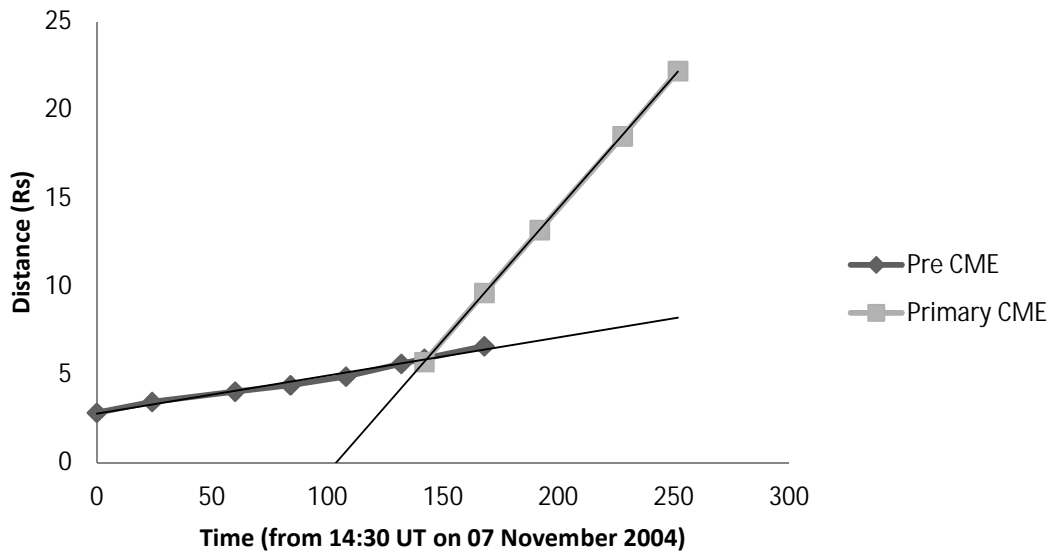


Fig. 4 Height-time diagram of pre and primary CMEs drawn together to show the interaction on 07 November 2004. The interaction of two CMEs occurred ~17:00 UT around a height of ~5 Rs.

The interaction height and interaction time are estimated from the height-time plots and they are listed in Table 2. Column 2-4 represent the date, time of first detection and

linear speed of primary CMEs. The interaction height, time and delay time between the onsets of pre and primary CMEs are given in column 5-7. Details of X-ray flares (class, Active Region number, location, duration and integrated flux) associated with the primary CMEs are given in column 8-12). The SEP intensity data (> 10 pfu) corresponding primary CMEs is given the last column. A distribution plot of interaction heights is shown in Figure 5. The range of interaction height is between 5 – 28Rs and mean interaction height of the events is found to be 15Rs. It is nearly similar to the mean interaction height of CMEs associated with SEP events (21 Rs) observed by Gopalswamy (2002) and mean interaction height of CMEs with DH type II events (18 Rs) determined by Prasanna and Shanmugaraju(2013). Also, delay between the onsets of pre and primary CMEs is calculated. The delay lies in the range 26-604 minutes with a mean value of 235mins.

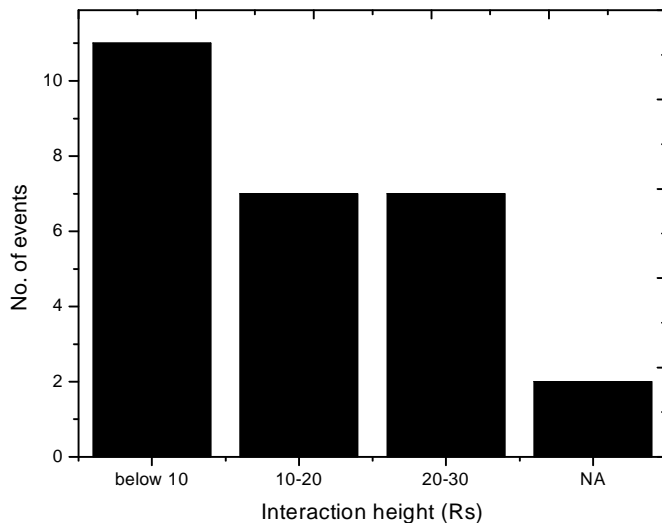


Fig. 5 Histogram plot shows the distribution of interaction height determined from the over-plotted height-time plots of pre and primary CMEs.

Similarly, the properties of all the pre and primary CMEs and their associated activities are obtained and their properties are analyzed further statistically. For example,

Figure 6 shows the distribution of speeds of pre and primary CMEs. It is seen that most of pre-CMEs have speed less than 1000km/s, whereas, many of the primary CMEs have speeds in the range 500 – 2000 km/s. The mean speed of the primary CMEs is 1361 km/s which is found to be more than twice the mean speed 523 km/s of pre-CMEs. This is similar to the mean speed of pre and primary CMEs reported by Gopalswamy et al.(2002) and Prasanna and Shanmugaraju (2013). Similarly the final observed distance (FOD) of primary CME is nearly twice the FOD of pre-CMEs. Most of the primary CMEs are halo CMEs, whereas, pre-CMEs have a lower mean width of 121 degrees.

Quite recently, Ding et al.(2013) reported the twin-CME scenario and large solar energetic particle events (SEPs) in solar cycle 23 using a set of fast CMEs ($v > 900$ km/s and width > 60 degrees) . They found four groups of events: (i) twin and (ii) single CMEs associated with large SEPs, (iii) twin and (iv) single CMEs not associated with large SEPs. Of 59 large SEP events, 43 and 16 events are found by them to be associated with twin and single CMEs, respectively. Also they reported that not all twin CMEs are associated with large SEP events. They suggested that the studies of the role of preceding flares are necessary to better understand the twin-CME scenario. Among 25 events in the present study, 9 events are listed in twin-CME category of Ding et al.(2013).

The X-ray flares associated with the primary CMEs are obtained from the Wind/WAVEs catalog and those associated with the pre-CMEs are obtained from the flare catalog by following certain time window of +/- one hour from the first appearance time of pre-CMEs. They are listed in Tables 2 and 3 for primary CMEs and pre-CMEs, respectively, along with their properties like flare class, duration and X-ray integrated flux. The number of C, M and X-class flares associated with the primary CMEs are 5, 10 and 12, respectively. While the flares associated with the primary CMEs are predominantly M and X-class flares, the flares associated with pre-CMEs are mostly C and M-class flares. This is in agreement with the recent results of Ding et al.(2013) where they showed that the mean strength of X-ray flares associated with pre-CMEs (C9.1) and primary CMEs (M9.6). The distributions of number of flares in each class are given in Figure 7. Flare duration is

estimated for both groups of flares associated with pre and primary CMEs. The mean value is found to be 55 min for primary CMEs, whereas, it is 36 min for pre-CMEs. It indicates that the flares associated with the primary CMEs are also of long duration flares (LDE flares).

The statistical values of mean, median and standard deviation of the properties of pre and primary CMEs are given in Table 4. From this table, it is also clear that the primary CMEs are much more energetic than the pre-CMEs. The flares associated with the pre-CMEs are of short duration with integrated flux nearly seven times less than that of primary-CMEs. Some of the events are found to be associated with major SEP proton events. From GOES proton data, we identified **9** major SEP events (proton flux intensity > 10 pfu) for which the SEP data are taken from the website

Table 4: Statistical properties of pre and primary CMEs and their associated flares

Properties	Pre-CMEs					Primary CMEs						
	Speed (km/s)	Width (deg)	FOD (Rs)	Flare duration (min)	Flare Integrated Flux ($\times 10^{-2}$ J/m ²)	Speed (km/s)	Width (deg)	FOD (Rs)	Int. Height (Rs)	Time Delay (min)	Flare Duration (min)	Flare Integrated Flux ($\times 10^{-2}$ J/m ²)
Mean	523	115	11	36	2	1361	274	22	15	235	55	21
Standard Deviation	440	116	8	28	3	493	113	5	8	167	44	30
Median	374	59	11	31	1	1393	360	23	14	211	41	7

www.umbra.nascom.nasa.gov/sep. From the analysis of the flare and SEP data, we found that the SEP intensity is related to the integrated X-ray flux of the flares associated with the

primary CMEs. Note that, Ding et al.(2013) reported neither the flare size nor CME speeds are the deciding factors of the size of proton peak intensity of the SEP events. Very recently, Joshi et al.(2013) analyzed extensively a single event on 23 January 2012 and found that the interaction of CMEs have important implications in producing large SEP events. It is also found that all the nine events associated with SEP are western side events and six of them are from northern region. Also for six events, the flares associated with primary CMEs have duration >25 min. The western region has good connectivity with the Earth. Gopalswamy et al.(2008) suggested for space weather applications that if a CME originating from the western hemisphere is accompanied by a DH type II burst, there is a high probability that it will produce an SEP event.

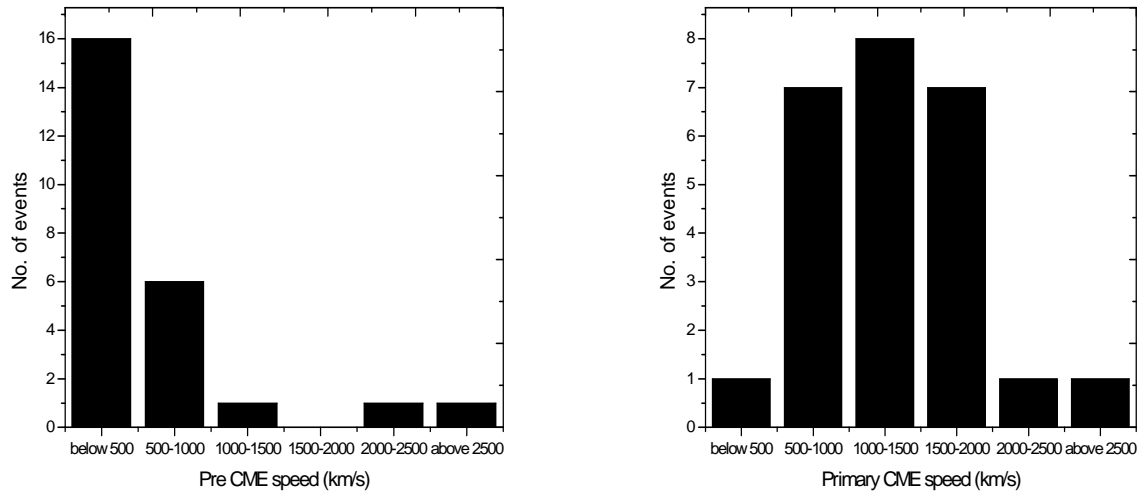


Fig 6 Histogram shows the distribution of speeds of pre and primary CMEs

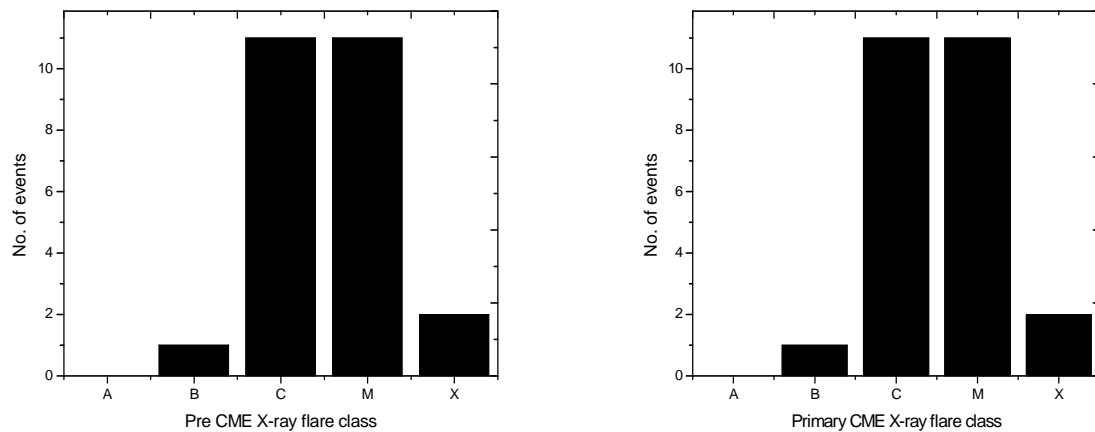


Fig 7 Histogram shows the distribution of X-ray flare class of pre and primary CMEs.

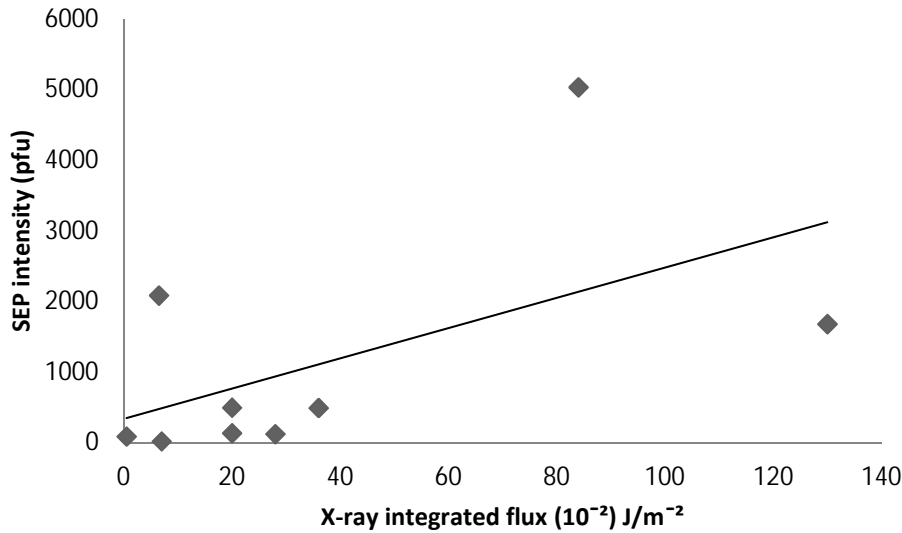


Fig 8 Distribution of SEP intensity and X ray integrated flux corresponding to the primary CMEs.

4 Conclusion

A set of 25 interacting CMEs ejected from the nearby active region in the same quadrant and associated with DH type II bursts are identified during the period 1997 – 2010, and their properties are analyzed. These events are collected based on several selection criteria. The pre and primary CMEs and their interactions are identified using LASCO images of SOHO and their height – time diagrams. Most of the interacting events associated with DH type II bursts occurred between the periods 2000-2006 which more number of energetic CMEs were ejected. The associated activities, such as, flares and SEPs are also investigated. Results from this analysis are:

i) Primary CMEs are much faster than the pre-CMEs and their X-ray flares are also stronger (M and X class) compared to the flares (M and C class) of pre-CMEs. The flares associated with primary CMEs are also of longer duration compared to the flares of pre-CMEs.

ii) From the observational data of speed and width of pre and primary CMEs, it is found that the pre-CMEs are found to be less energetic than the primary CMEs.

iii) While the primary CMEs are tracked up to the end of LASCO field of view (30Rs), most of the pre-CMEs can be tracked up to < 26Rs.

iv) The mean values of interaction height and delay between the onsets of pre and primary CMEs are found to be 15 Rs and 235 min.

v) For the 9 events associated with major SEPs, the SEP intensity is found to be related to the integrated X-ray flux of the flares associated with the primary CMEs. These events are from the western region of the Sun.

Acknowledgement

We would like to thank Prof. P.K. Manoharan (Radio Astronomy Centre, NCRA-TIFR, Ooty, India) for constructive discussions and the referee for his comments. The authors gratefully acknowledge the data support provided by various online data centers of NOAA and NASA. We would like to thank the Wind/WAVES team for providing the type II catalogs. The CME catalog we have used is provided by the Center for Solar Physics and Space Weather, The Catholic University of America in cooperation with the Naval Research Laboratory and NASA. Also we thank the umbra and NASCOM team for providing Solar Energetic particle data. The major research grant No. 42 – 845 / 2013 (SR) to A.S. from University Grants Commission, Govt. of India is kindly acknowledged.

References

Ding, L., Jiang, Y., Zhao, L., and Li, G.: *Astrophys. J.* 763 30 (2013)

Gopalswamy, N., Yashiro, S., Kaiser, M.L., Howard, R.A., Bougeret, J.L.: *J. Geophys. Res.* 106, 29219 (2001a)

Gopalswamy, N., Yashiro, S., Kaiser, M.L., Howard, R.A., Bougeret, J.L.: *Astrophys. J.* 548, L91 (2001b)

Gopalswamy, Yashiro S., Michalek, G., Kaiser, M. L., Howard, R. A., Reames, D. V., Leske, R. and Von Rosenvinge, T.: *Astrophys. J.*, 572:L103, (2002)

Gopalswamy, N., Aguilar-Rodriguez, E., Yashiro, S., Nunes, S., Kaiser, M.L., Howard, R.A.: *J. Geophys. Res.* 110, 12S07 (2005)

Gopalswamy, N., Yashiro, S., Akiyama, S., Makela, P., Xie, H., Kaiser, M.L., Howard, R.A., Bougeret, J.-L.: *Ann. Geophys.* 26, 3033(2008)

Harrison, R.: *Astron. Astrophys.*, 162, 283(1986)

Harrison, R.: *Astron. Astrophys.*, 304, 585(1995)

Jing, J., et al. : *Astrophys. J.* 620, 1085(2005)

Joshi, N.C. et al. : *Adv. Space Res.* 52, 1 (2013)

Liu, Y.D., Luhmann, J.G., Christian, M.: *The Astrophys. J. Lett.*, 746, 2, L15, 7(2012).

Lugaz N., Manchester, W.B., Gombosi, T.I.: *Astrophys. J.* 634, 651(2005)

Manoharan, P.K., Gopalswamy, N., Yashiro, S., Lara, A., Howard, R.A., Michalek, G.: *J. Geophys. Res.* 109, A06109 (2004)

Martínez, O., Juan, C., Raftery, C.L., Bain, H.M., Liu, Y., Krupar, V., Bale, S., Krucker, S.: *Astrophys. J.* 748, 66 (2012)

Prasanna Subramanian, S., Shanmugaraju, A. : *Astrophys. and Space Sci.*, 344(2), 305 (2013)

Temmer, M., Vrsnak, B., Rollett, T., et al.: *Astrophys. J.* 749, 57(2012)

Yashiro, S., Gopalswamy, N., Michalek, G., St. Cyr, O. C., Plunkett, S. P., Rich, N. B., and Howard, R. A.: *J. Geophys. Res.*, 109, A07105 (2004)

Yashiro, S., Gopalswamy, N.: *Universal Heliophysical Processes*, eds., 233(2008)

Yan, X.L., Qu, Z.Q., Kong, D.F.: *R. Astron. Soc.*, 414(7), 2803(2011).